Nanoscale

PAPER

View Article Online
View Journal | View Issue

Cite this: *Nanoscale*, 2014, **6**, 3934

Multipole plasmon resonances in self-assembled metal hollow-nanospheres

Jun Yin,[ab] Yashu Zang,[a] Binbin Xu,[c] Shuping Li,[a] Junyong Kang,[a] Yanyan Fang,[b] Zhihao Wu*[b] and Jing Li*[a]

Received 5th August 2013
Accepted 29th September 2013

DOI: 10.1039/c3nr04106a

www.rsc.org/nanoscale

Recently, multipole plasmonic mode resonances in metal hollow structures, such as dipole, quadrupole, and octupole modes, have been widely investigated by researchers with the aim for potential applications in bio-sensing, fluorescence, nanolasers or nonlinear nano-photonics. Here, in this work, the multipole plasmon resonances in self-assembled metal hollow-nanospheres (HNSs) are theoretically and experimentally demonstrated and the hot spots originating from the higher order mode plasmonic resonance and interparticle coupling effect are proposed to be used for Raman scattering enhancements. Dipole, quadrupole, octupole and hexadecapole mode plasmonic resonances were clearly resolved in the extinction spectra of these Ag HNS arrays showing good agreement with the theoretical simulation results. Strong regular hot spots were obtained around the surface and in the gaps of the Ag HNSs through the higher order mode plasmonic resonances and corresponding interparticle coupling effect between the HNSs. Maximum local field intensity was accomplished by optimizing the size of as well as the coupling distance between the HNSs and then it was applied to SERS sensing. Raman mapping also demonstrated these self-assembled plasmonic cavity arrays to be a stable and uniform SERS-active substrate.

Introduction

Surface plasmon based surface-enhanced Raman scattering (SERS)[1] is a leading non-destructive technique that helps to extend the sensitivity of Raman spectroscopy to the level of a single molecule.[2,3] Generally, the strongly enhanced local near-field originating from the surface plasmon resonance (SPR) effect on the metal nanostructures is the main mechanism for surface plasmon based SERS.[4] In recent years, a large local near-field enhancement generated from the local surface plasmon resonance (LSPR) effect in a specific region around or its inter-coupling effect between metal NPs, which is defined as a 'hot spot', has drawn researchers' attention and been widely proposed and demonstrated for single molecule level detection.[5–7] Due to the special geometries with controllable morphologies and parameters,[8–10] adjustable plasmon bands[9,10] and resonance modes[11–15] can be easily realized in metal hollow nano-structures. Thus, they have been extensively studied and applied to highly sensitive SERS sensing given the highly localized near-field[7,15] and the corresponding regular hot spots around the nanoparticles.[16–19] M. A. Mahmoud and his co-workers have symmetrically investigated both the surface plasmon resonance and the coupling properties of gold hollow nanocages by optimizing the size and shell thickness aiming for highly sensitive SERS detection.[18]

Multipole SPR modes on gold or silver nanostructures, such as core shells,[7,8,20] nanoprisms,[21] nanorods[22,23] or spherical particles,[24,25] have been observed in previous studies. Recently, these multipole plasmonic resonance modes in metal shells or cavity structures have gained much renewed attention due to the potential applications in bio-sensing,[26] fluorescence,[27] nanolasers,[28,29] or nonlinear nano-photonics.[30] Commonly, a highly localized electromagnetic field can be obtained in or on the plasmonic cavities through the resonances in multipole modes, which have been proposed to create high quality (Q) factor plasmonic resonators[31,32] or ultra-small-mode-volume devices, *e.g.* nanolasers, surface plasmon amplification by stimulated emission of radiation (SPASER), *etc.*[28,29] Additionally, by using the highly localized electromagnetic fields on the exterior surface of a plasmonic resonator, in which plasmonic whispering-gallery mode (WGM) resonance happens, the cavity can be potentially used as a WGM resonator based bio-sensor with a high sensitivity of up to 500 nm per refraction index unit, and wide detection range.[26]

Here, in this work, multipole plasmon resonances were realized in the self-assembled Ag hollow-nanospheres (HNSs).

[a]*Department of Physics/Pen-Tung Sah Institute of Micro-Nano Science and Technology, Xiamen University, Xiamen, 361005, China. E-mail: lijing@xmu.edu.cn; Fax: +86-592-2187196; Tel: +86-592-2181340*

[b]*Wuhan National Laboratory for Optoelectronics, School of Optical and Electronic Information, Huazhong University of Science and Technology, Wuhan, 430074, China. E-mail: zhihao.wu@mail.hust.edu.cn; Fax: +86-27-87793035; Tel: +86-27-87793024*

[c]*College of Chemistry and Chemical Engineering, Xiamen University, Xiamen, 361005, China*

Benefiting from higher order plasmonic resonances, a highly localized near-field around the surface and hot spots generated by the inter-coupling effect in the gaps were obtained within the HNS arrays, which were then demonstrated to be an ideal SERS substrate by taking advantage of these enhanced local fields. The large scale two-dimensional (2D) Ag HNS arrays were fabricated using the self-assembled polystyrene (PS) nanospheres as the template with its size and gaps adjusted by employing reactive-ion etching (RIE) on the template. Dipole, quadrupole, octupole and hexadecapole mode plasmonic resonances are distinguishably resolved from the extinction spectra showing good agreement with the simulated spectra and near-field distributions. According to the FDTD simulation results, highly localized electromagnetic field distribution and strong regular hot spots were obtained around or in the gaps between the Ag HNSs through the interparticle coupling effect, which are believed to be responsible for the highly sensitive SERS performance on the Ag HNS arrays with the optimized size and gaps. Further Raman mapping from this metal hollow structure evidences these periodic plasmonic cavity arrays to be a stable and uniform SERS-active substrate.

Experimental details

The Ag HNS arrays were fabricated using the colloidal template method[33] as described in our previous work.[34] Commercial PS nanospheres purchased from Thermo Scientific with a diameter of 500 nm were used as template materials to fabricate the metal HNS arrays. The fabrication processes are schematically shown in Fig. 1. Briefly, a self-assembled PS nanosphere monolayer on a silicon or sapphire substrate was used as the template. RIE was introduced to manipulate the size and separation of the PS nanospheres in the template by adjusting the O_2 plasma etching time. After sputtering deposition of a thin Ag film on the template, the PS nanospheres in the core were etched by tetrahydrofuran (THF) solution and the samples were dried in N_2 gas. Eventually, Ag HNS arrays were produced on the substrates.

The morphologies and structure properties of the samples were investigated using a Hitachi S-4800 field-emission SEM and JEM-2100 HRTEM equipped with an energy dispersive X-ray spectrum (EDS) analyzer. The crystallinity of the samples was characterized using a Panalytical X'pert PRO XRD with Cu-Kα radiation ($\lambda = 1.5406$ Å) in a 2θ range of 20–60°. Transmission spectra of all the samples on sapphire substrates were measured using a UV-Vis-NIR spectrophotometer (Varian, UV-Vis-NIR Cary 5000). A commercial FDTD simulation package (FDTD Solutions, Lumerical Solutions Inc.) was used for calculating the extinction spectra and near field distribution of the metal HNSs. The SERS properties were characterized by confocal Raman spectroscopy (Renishaw inVia Raman Microscope) with a 532 nm laser excitation source. Rhodamine 6G (R6G) was used as the SERS analysis probe and dissolved in DI water until the concentration of 10^{-5} M. 2 μL suspension was dropped on the substrate and naturally dried in air before SERS measurements. The Raman mapping was performed on a confocal Raman imaging system (WITec Confocal Raman Microscope Alpha 300) equipped with a 488 nm laser excitation source.

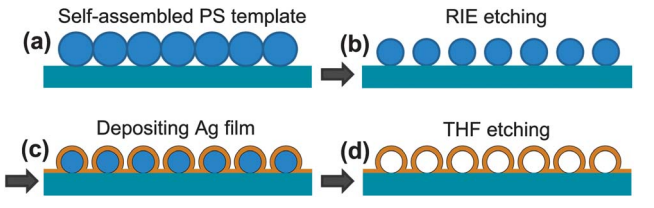

Fig. 1 Schematic illustration of the fabrication processes of Ag HNS arrays: (a) self-assembled PS nanosphere monolayer on a silicon or sapphire substrate; (b) RIE on a template to adjust the size and gaps of the PS nanosphere arrays; (c) Ag film deposition on the template; (d) the PS core removal by THF solvent.

Results and discussion

Large area hexagonally packed Ag HNS arrays in a monolayer were successfully fabricated using the colloidal template method as shown in Fig. 2a. The size and distribution of the Ag HNSs have been well controlled by employing the RIE on the PS templates as shown in Fig. 2b–e, which have been etched by O_2 plasma for 0 s, 30 s, 60 s and 90 s and thus with the corresponding core diameter of the fabricated Ag HNSs measured to be about 450, 420, 400 and 380 nm, respectively. Because of the further reduction of the size of the PS nanospheres induced by the electron bombardment during the RF magnetron sputtering process, the produced actual size of the Ag HNS arrays would be much smaller than the original PS nanosphere on the template

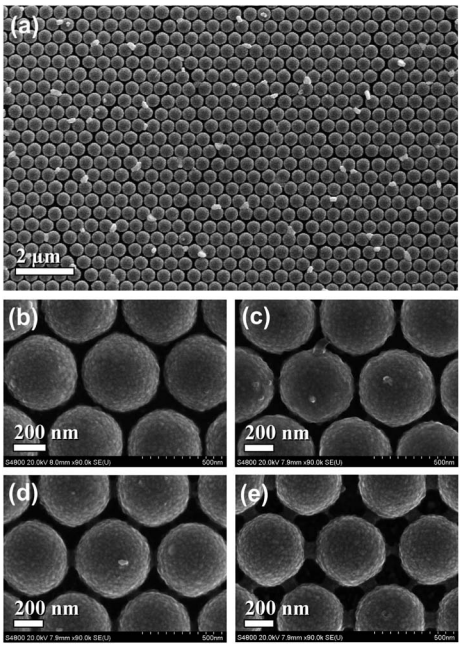

Fig. 2 SEM images of (a) as-fabricated large area Ag HNS arrays, and (b–e) Ag HNS arrays with the size and gap adjusted by RIE on PS templates for 0, 30, 60 and 90 s, respectively.

after the RIE. Therefore, the diameter of the Ag HNSs on the sample with 0 s of RIE is ~450 nm, which is smaller than the original diameter of 500 nm for PS nanospheres in the template, so do other samples. Understandably, the gaps between the Ag HNSs can also be adjusted by controlling the RIE time.

Clear hollow structures can be visualized from the TEM images of a randomly selected single Ag HNS in Fig. 3a and b. The EDS pattern shown in Fig. 3c demonstrates that the PS template in the core has been removed completely by THF etching, resulting in a hollow structure. The selected area electron diffraction (SAED) pattern taken from the surface of the Ag HNS in (b) infers a polycrystalline structure of the Ag shell layer, as shown in the inset of Fig. 3c. According to the measured interplanar lattice spacing from the SAED pattern (0.236 nm and 0.204 nm) and JCPDS card no. 04-0783, the diffraction mainly comes from the (111) and (200) planes of face-centred cubic (FCC) Ag. Fig. 3d shows the HRTEM image of Ag nanograins on the shell layer and the interplanar lattice spacing is measured to be around 0.236 nm, which corresponds to the (111) plane of FCC Ag. The crystallinity of the samples was also confirmed by the XRD pattern shown in Fig. 3e. The dominant diffraction peaks at 38.1° and 44.3° (2θ) are attributed to the FCC Ag (111) and (200) plane diffraction, respectively, which are in good agreement with the TEM characterization.

In order to investigate the SPR properties of the fabricated Ag HNS arrays, the extinction spectra were measured on a sapphire substrate and then compared with the FDTD simulation results.

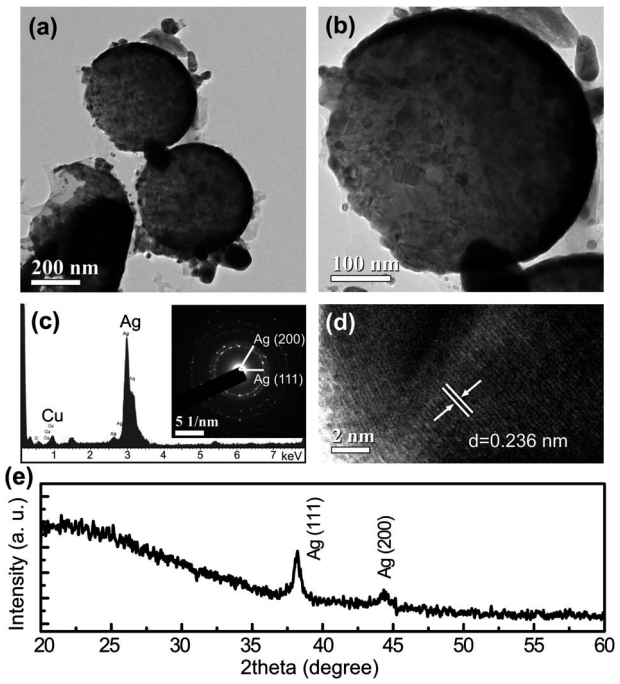

Fig. 3 TEM and XRD characterizations of the as-fabricated Ag HNS: TEM images of Ag HNSs (a) at lower and (b) higher magnifications; (c) EDS pattern taken from the surface of the Ag HNS in (b) with the corresponding SAED pattern shown in the inset; (d) HRTEM image of Ag nanograins on the surface of Ag HNS; (e) XRD pattern of Ag HNS arrays on a silicon substrate.

Fig. 4a shows the typical extinction spectrum of the Ag HNS arrays produced on the PS template etched by O_2 plasma for 30 s. Several distinguished resonance peaks can be resolved at the wavelengths of about 380, 445, 540, 815 and 1330 nm as marked with grey arrows. With the aim to gain the origin of these resonance peaks, the extinction and scattering spectra of a single Ag HNS were simulated as shown in Fig. 4b. The resolved peaks located at the wavelengths of about 410, 480, 608, 808 and 1340 nm match well with those in the experimental results except for some red shifts, which should be reasonably due to the non-homogeneous shell thickness in experimentally produced Ag HNS arrays and the inter-coupling effect between HNSs.[16,35] It can also be found that the experimentally characterized extinction intensity for the higher order plasmon resonances is not as strong as that in the theoretically calculated one, while the dipole mode resonance shows relatively higher experimental intensity. Due to the extensively surface topography dependent properties of higher order plasmon resonances on the metal shell structure,[36] the higher order plasmon modes would be suppressed rapidly when a rough surface and imperfect spherical shape present on the actual metal shell structure fabricated using the sputtering method for metal film deposition in this work. So the obtained higher order plasmon resonance mode is not as strong as the dipole mode in the experimental extinction results. Since the total extinction cross-section is contributed by both the scattering and absorption cross-sections, it is certain that the scattering part in this Ag hollow structure generally induced by the SPR effect is mainly participating in the extinction process.

It is well accepted that the spectral features of the LSPR are determined by the relative dimensions of the particle in relation to the electromagnetic radiation at a specific wavelength.[37,38] When the dimensions of nanoparticles are much smaller than the wavelength of light, such as Ag nanoparticles with size ranging from 10 to 50 nm, the particles would exist in a uniform electromagnetic field. As a result, all electrons in the metal experience roughly the same phase of the incident electromagnetic field producing only a dipole type of oscillation. However, across a larger size nanoparticle, the field becomes non-uniform and light cannot polarize on the particle homogeneously, which results in phase retardation of the applied field inside the material. As a consequence, broadening in the dipole surface plasmon related resonance peak is observed in larger particles along with the appearance of higher order multipole resonances (quadrupole, octupole, *etc.*) as seen in Fig. 4a. In order to evaluate the resonance states for each peak resolved in the extinction spectra of Fig. 4b, the near-field distribution and charge density at each resonance wavelength were simulated as shown in Fig. 4c and d. From the calculated near-field distribution, it can be inferred that the resonance peaks identified in Fig. 4b originate from the series modes of LSPR: dipole, quadrupole, octupole and hexadecapole modes, respectively, so do the resonances in Fig. 4a. The charge density distribution calculated at each corresponding resonance wavelength as shown in Fig. 4d shows distinct eight, six, four and two charge lobes, which evidently demonstrates the plasmonic resonance characteristics of hexadecapole, octupole,

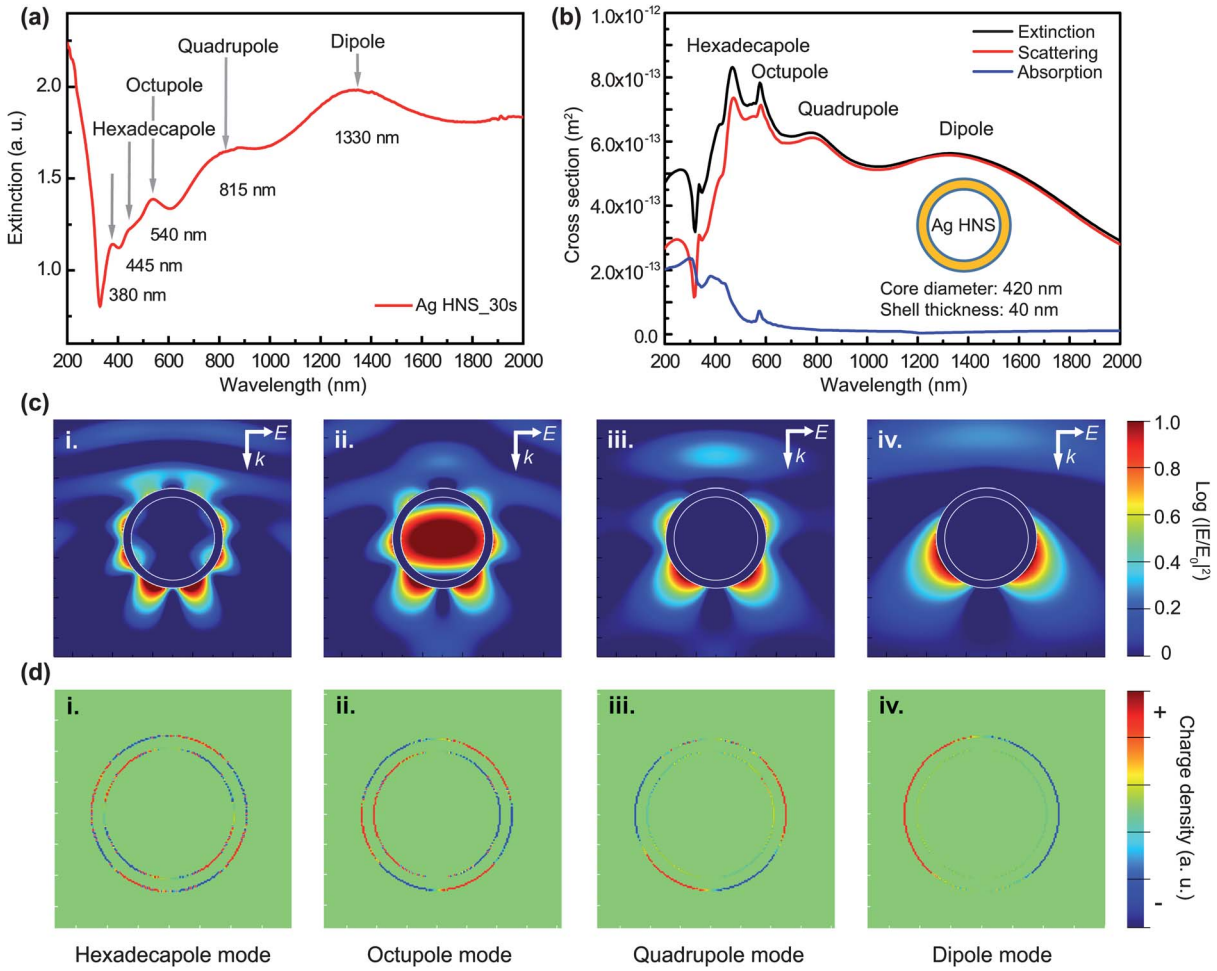

Fig. 4 (a) Extinction spectrum of the Ag HNS arrays on a sapphire substrate using the PS template by RIE for 30 s; (b) simulated extinction, scattering and intrinsic absorption cross-sections for a single Ag HNS with a core diameter of 420 nm and shell thickness of 40 nm; calculated (c) near-field distributions and (d) charge density distributions around a single Ag HNS under the series of resonance wavelengths consistent with those marked in (b). The parameters of the Ag HNS are the same as those in (b) and the light incidence direction and polarization are shown in the patterns.

quadrupole and dipole modes.[39] Due to the specific geometry of the metal hollow structure, higher order LSPR modes besides the normal dipole and quadrupole modes can exist, which exhibit a strong and highly localized electromagnetic field near the hollow structure. In this work, the strongly localized near-field around the Ag HNSs and the corresponding hot spots generated by the higher order resonances around or the inter-coupling effect between those metal hollow plasmonic nanostructures can be potentially proposed for Raman scattering enhancement.

As shown in Fig. 2b–e, the size and gaps of the fabricated Ag HNS arrays can be successfully controlled by the RIE on templates to adjust the size of PS nanospheres. The corresponding extinction spectra of those fabricated Ag HNS arrays in different core diameters and gaps were measured and are shown in Fig. 5a, in which an obvious blue shift in the lower order SPR peaks, *e.g.* quadrupole mode, can be observed. As systematically investigated in the previous studies,[9,40] the aspect ratio (outer diameter to shell thickness) of the metal shell structure plays an important role in the plasmon bands, where the resonance peaks would undergo blue shift when the size or the aspect ratio decreases (shell thickness kept constant) as the plasmon oscillation increases in energy. So, the blue shift of the lower order SPR peaks can be understandably attributed to the decrease of the Ag HNS size or the aspect ratio. On the other hand, it can be noticed that the higher order SPR peaks, such as octupole or hexadecapole modes, are not sensitive to the size change in these Ag hollow nanostructures. As displayed in Fig. 5b, the simulated extinction spectra match well with the experimental results: the resonance peaks in lower order modes obviously shift to shorter wavelength as the diameter of the Ag HNSs decreases, while the higher order mode resonances shift slightly. The grey arrows marked in the figure indicate the shift tendency for these multipole SPR modes.

Fig. 6a shows the simulated near-field distribution for the Ag HNS arrays on a silicon substrate in the core diameters consistent with those of 450, 420, 400 and 380 nm in the above fabricated samples. The incident light is chosen at a wavelength of 532 nm, which is the same with the laser excitation line in later SERS characterization. It can be found that a strong local

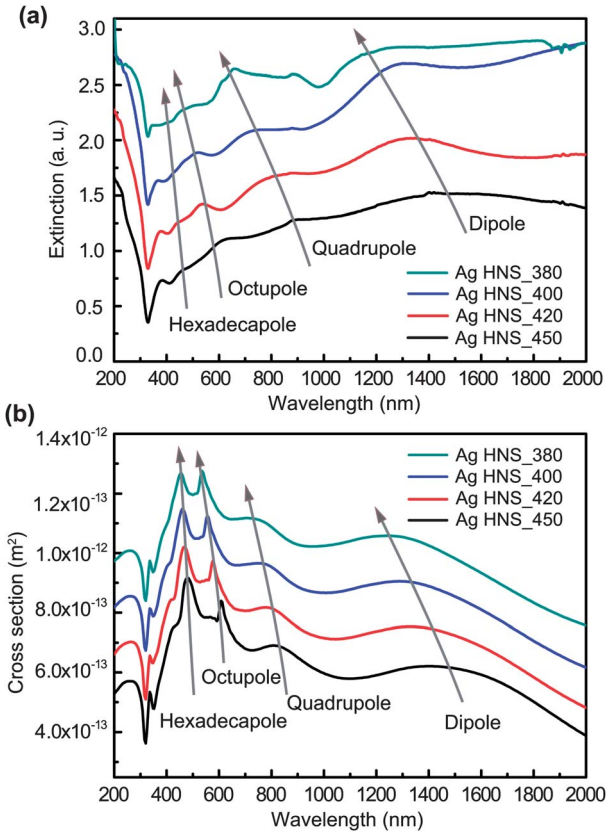

Fig. 5 (a) Extinction spectra of the Ag HNS arrays with a core diameter of 450, 420, 400 and 380 nm fabricated on different PS templates with changing the O_2 plasma etching time for 0 s, 30 s, 60 s and 90 s, separately; (b) FDTD simulated extinction spectra for a single Ag HNS in the core diameters consistent with those in the samples of (a).

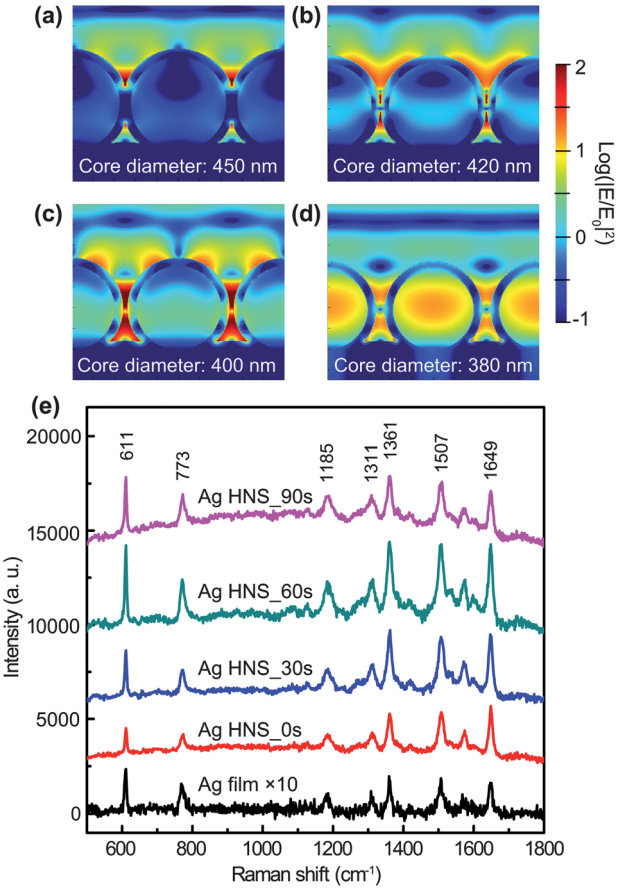

Fig. 6 (a) Simulated near-field distribution for the Ag HNS arrays on a silicon substrate with core diameters of 450, 420, 400 and 380 nm, which are the same as the measured values in as-fabricated samples. (b) SERS characterization on the fabricated Ag HNS array samples using R6G as the analyte and compared with the bare Ag film substrate. The concentration of R6G is 1.0×10^{-5} M and the laser power was set to be 0.5 mW.

field near the gaps between Ag HNSs could be obtained in each sample, while it has a maximum value in the Ag HNS arrays optimized with a core diameter of 400 nm and interval space of 20 nm. This size and gap dependent local field, suggested to be originated from the strong inter-coupling effect between metal Ag HNSs, is commonly known as a hot spot.[16] As the hot spot mainly arises from a few nanometers in the gap, a stronger coupling effect was expected when the interval space between the Ag HNSs emerges after reducing the size of the PS nanosphere template by RIE for a certain time. So the sample with a core diameter of 400 nm shown in Fig. 6c exhibits the strongest local field in the gaps. While, when the core diameter further reduces, the coupling effect is suppressed rapidly due to the enlarged gap distance, so the weak local field is revealed in the gap for the sample with a core diameter of 380 nm shown in Fig. 6d. Additionally, around the top surface of these optimized HNSs an intensive localized field can be resolved compared to the spreading field with lower intensity on the larger sized Ag HNSs, which is suggested to be caused by the higher order plasmonic resonance modes, mainly octupole mode, given the incident light at a wavelength of 532 nm.

The SERS characterizations performed on these samples using the R6G as the analyte further evidence this hot spot effect as shown in Fig. 6e. The characterized Raman bands located at 611, 773, 1185, 1311, 1361, 1507 and 1649 cm^{-1} marked in the spectra belong to the typical Raman vibrations of R6G and match well with the reported results in the literature.[41] Compared with the bare Ag film on a silicon substrate, stronger Raman signals can be obtained on all the hollow structure samples, which is understandably caused by the generation of hot spots in those HNS array structures. The SERS enhancement factor (EF) was estimated by $(I_{SERS}/I_{NR})(N_{NR}/N_{SERS})$,[42] where I_{SERS} and I_{NR} represent the SERS intensities of the Raman band for R6G adsorbed on the metal shells and normal Raman (NR) scattering intensity measured for R6G absorbed on the bare silicon substrate, respectively, whereas N_{SERS} and N_{NR} are the corresponding number of R6G molecules which contribute to the Raman spectra. I_{SERS} and I_{NR} were measured at 611 cm^{-1}, and N_{NR}/N_{SERS} were calculated on the basis of the prepared concentration of R6G species and the sampling areas. As estimated using the above method, SERS enhancements of 0.48×10^5, 0.90×10^5, 1.6×10^5 and 1.1×10^5 orders of magnitude were obtained for the Ag HNS array samples with a core diameter of 450, 420, 400 and 380 nm, respectively. Notably, the

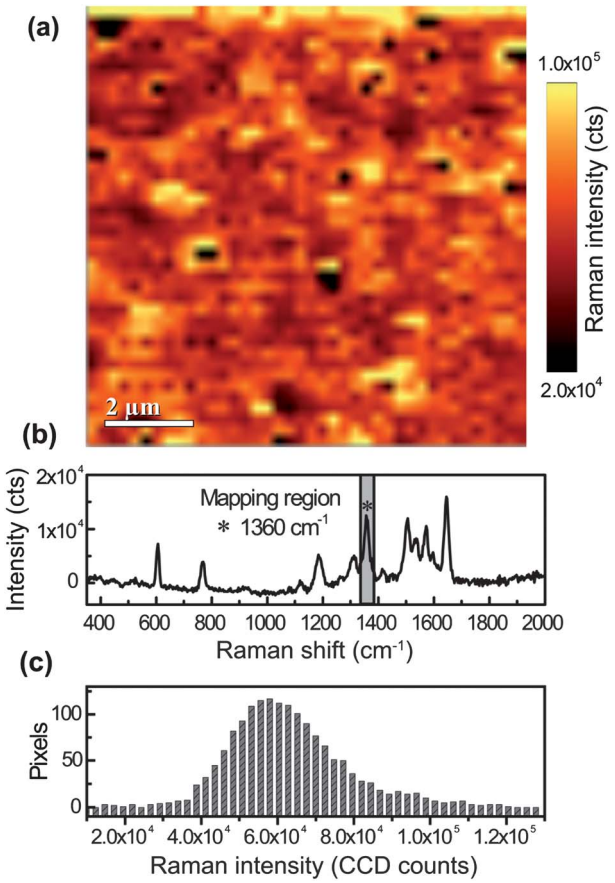

Fig. 7 (a) Raman mapping image on the Ag HNS arrays (10 μm × 10 μm) at the Raman shift of 1360 cm^{-1}, (b) the corresponding Raman spectrum and (c) histogram of Raman intensities in the Raman mapping of (a). All spectra in the considered region perform a background subtraction before integration calculation.

largest enhancement is accomplished on the optimized Ag HNS arrays with a core diameter of 400 nm, which is consistent with the calculation results as discussed above. Therefore, the Ag HNS array is suitable as SERS substrates given its simple fabrication process and handy size and gap controlling.

In order to evaluate the SERS uniformity, Raman mapping was performed on the fabricated Ag HNS arrays in a large area (10 μm × 10 μm) at the Raman shift of 1360 cm^{-1}, as shown in Fig. 7a. Each pixel in the confocal Raman mapping images represents the integral Raman intensity near 1360 cm^{-1} in the area of interest (1320–1400 cm^{-1}) as marked in Fig. 7b. The mapping image together with the histogram of Raman intensities shown in Fig. 7c demonstrates that uniform SERS signals can be obtained on this self-assembled Ag HNS array substrate.

Conclusions

Multipole surface plasmon resonances: dipole, quadrupole, octupole and hexadecapole modes were observed in self-assembled metal hollow-nanosphere arrays and further demonstrated by the extinction spectra and FDTD simulations. The highly localized near-field on the surface of the Ag HNS arrays due to the multipole mode plasmonic resonances and the periodic hot spots generated from the high order LSPR and its interparticle coupling effect make these metal nanostructure arrays a suitable SERS substrate for bio-sensing. In this manner, a sensitive SERS performance was accomplished on the Ag HNS array substrate with optimized size and gaps. Further Raman mapping characterization results on these metal HNS arrays in a large area evidently confirm that these periodic plasmonic hollow cavity arrays could be used as a stable and uniform SERS-active substrate with wide applications in bio-sensing, analytical chemistry and so on. Furthermore, broadband light manipulation, such as light trapping, from the UV to the near-infrared region can also be potentially achieved by using the multipole surface plasmon resonances in this metal hollow spherical structure.

Acknowledgements

This work is financially supported by the MOST of China under the 973 programs (2009CB930704), National Natural Science Foundation of China (61106118), Science and Technology Project of Fujian Province of China (2013H0046), Natural Science Foundation of Fujian Province of China (2011J01362), and Fundamental Research Funds for the Central Universities (2011121026).

Notes and references

1 M. G. Albrecht and J. A. Creighton, *J. Am. Chem. Soc.*, 1977, **99**, 5215.
2 S. M. Nie and S. R. Emory, *Science*, 1997, **275**, 1102.
3 K. Kneipp, Y. Wang, H. Kneipp, L. T. Perelman and I. Itzkan, *Phys. Rev. Lett.*, 1997, **78**, 1667.
4 H. R. Raether, *Surface Plasmons on Smooth and Rough Surfaces and on Gratings*, Springer, 1988.
5 N. J. Halas, S. Lal, W. S. Chang, S. Link and P. Nordlander, *Chem. Rev.*, 2011, **111**, 3913.
6 L. Shao, K. C. Woo, H. J. Chen, Z. Jin, J. F. Wang and H. Q. Lin, *ACS Nano*, 2010, **4**, 3053.
7 M. Rycenga, X. Xia, C. H. Moran, F. Zhou, D. Qin, Z. Y. Li and Y. Xia, *Angew. Chem., Int. Ed.*, 2011, **50**, 5473.
8 H. Wang, D. W. Brandl, P. Nordlander and N. J. Halas, *Acc. Chem. Res.*, 2007, **40**, 53.
9 S. Pattanayak, A. Priyam and P. Paik, *Dalton Trans.*, 2013, **42**, 10597.
10 A. Priyam, N. M. Idrisa and Y. Zhang, *J. Mater. Chem.*, 2012, **22**, 960.
11 E. Prodan, C. Radloff, N. J. Halas and P. Nordlander, *Science*, 2003, **302**, 419.
12 L. J. Sherry, S. H. Chang, G. C. Schatz, R. P. Van Duyne, B. J. Wiley and Y. N. Xia, *Nano Lett.*, 2005, **5**, 2034.
13 H. Minassian, K. Madoyan and A. Melikyan, *Plasmonics*, 2012, **7**, 745.
14 A. M. Schwartzberg, T. Y. Olson, C. E. Talley and J. Z. Zhang, *J. Phys. Chem. B*, 2006, **110**, 19935.
15 A. M. Schwartzberg, T. Y. Oshiro, J. Z. Zhang, T. Huser and C. E. Talley, *Anal. Chem.*, 2006, **78**, 4732.

16 S. K. Ghosh and T. Pal, *Chem. Rev.*, 2007, **107**, 4797.
17 H. N. Xie, I. A. Larmour, W. E. Smith, K. Faulds and D. Graham, *J. Phys. Chem. C*, 2012, **116**, 8338.
18 M. A. Mahmoud, B. Snyder and M. A. El-Sayed, *J. Phys. Chem. C*, 2010, **114**, 7437.
19 F. Hao, Y. Sonnefraud, P. Van Dorpe, S. A. Maier, N. J. Halas and P. Nordlander, *Nano Lett.*, 2008, **8**, 3983.
20 J. W. Liaw and C. Y. Jiang, *Plasmonics*, 2012, **7**, 745.
21 J. E. Millstone, S. Park, K. L. Shuford, L. D. Qin, G. C. Schatz and C. A. Mirkin, *J. Am. Chem. Soc.*, 2005, **127**, 5312.
22 E. K. Payne, K. L. Shuford, S. Park, G. C. Schatz and C. A. Mirkin, *J. Phys. Chem. B*, 2006, **110**, 2150.
23 R. B. Jiang, H. J. Chen, L. Shao, Q. Li and J. F. Wang, *Adv. Mater.*, 2012, **24**, OP200.
24 A. S. Kumbhar, M. K. Kinnan and G. Chumanov, *J. Am. Chem. Soc.*, 2005, **9**, 12445.
25 J. Rodríguez-Fernández, J. Pérez-Juste, F. J. García de Abajo and L. M. Liz-Marzán, *Langmuir*, 2006, **22**, 7007.
26 Y. F. Xiao, C. L. Zou, B. B. Li, Y. Li, C. H. Dong, Z. F. Han and Q. H. Gong, *Phys. Rev. Lett.*, 2010, **105**, 153902.
27 C. H. Cho, C. O. Aspetti, J. Park and R. Agarwal, *Nat. Photonics*, 2013, **7**, 285.
28 C. Z. Ning, *Phys. Status Solidi B*, 2010, **247**, 774.
29 M. I. Stockman, *Nat. Photonics*, 2008, **2**, 327.
30 Y. Zhang, T. Q. Jia, S. A. Zhang, D. H. Feng and Z. Z. Xu, *Opt. Express*, 2012, **20**, 2924.
31 B. Min, E. Ostby, V. Sorger, E. Ulin-Avila, L. Yang, X. Zhang and K. Vahala, *Nature*, 2009, **457**, 455.
32 C. Y. A. Ni, S. W. Chang, D. J. Gargas, M. C. Moore, P. D. Yang and S. L. Chuang, *IEEE J. Quantum Electron.*, 2001, **47**, 245.
33 F. Caruso, R. A. Caruso and H. Möhwald, *Science*, 1998, **282**, 1111.
34 J. Yin, Y. S. Zang, C. Yue, Z. M. Wu, S. T. Wu, J. Li and Z. H. Wu, *J. Mater. Chem.*, 2012, **22**, 7902.
35 K. H. Su, Q. H. Wei and X. Zhang, *Nano Lett.*, 2003, **3**, 1087.
36 H. Wang, G. P. Goodrich, F. Tam, C. Oubre, P. Nordlander and N. J. Halas, *J. Phys. Chem. B*, 2005, **109**, 11083.
37 K. L. Kelly, E. Coronado, L. L. Zhao and G. C. Schatz, *J. Phys. Chem. B*, 2003, **107**, 668.
38 U. Kreibig, B. Schmitz and H. D. Breuer, *Phys. Rev. B: Condens. Matter Mater. Phys.*, 1987, **36**, 5027.
39 F. Hao, E. M. Larsson, T. A. Ali, D. S. Sutherland and P. Nordlander, *Chem. Phys. Lett.*, 2008, **458**, 262.
40 A. M. Schwartzberg, T. Y. Olson, C. E. Talley and J. Z. Zhang, *J. Phys. Chem. B*, 2006, **110**, 19935.
41 H. Watanabe, N. Hayazawa, Y. Inouye and S. Kawata, *J. Phys. Chem. B*, 2005, **109**, 5012.
42 R. P. Van Duyne, J. C. Hulteen and D. A. Treichel, *J. Chem. Phys.*, 1993, **99**, 2101.